Journal of the European Ceramic Society **17** (1997) 1475–1483

PII: S0955-2219(97)00007-1
0955-2219/97/$17.00

Sol–Gel Control of Matrix Net-Shape Sintering in 3D Fibre Reinforced Ceramic Matrix Composites

Ph. Colomban* & M. Wey

ONERA, Direction des Matériaux, BP 72, 92322 Chatillon Cedex, France

(Received 4 October 1996; revised version received 26 November 1996; accepted 2 December 1996)

Abstract

The origin of thermochemical degradation of 3D reinforced ceramic matrix composites has been analysed by dilatometry, pore-size distribution and electron microscopy and correlated to the cracking arising from the matrix shrinkage in an invariant 3D fibre network. The matrix shrinkage of an alumina matrix composite has been delayed up to a higher temperature (+200°C) by post-infiltration with pure alkoxide which was subsequently in situ *hydrolysed, polycondensed and pyrolysed. Mechanical strength of the composites has been increased four times by optimizing alkoxides. The tensile and flexural mechanical strengths of these alumina matrix composites are similar to those obtained from SiC matrix composites prepared by the CVI process using the same 3D carbon preform. © 1997 Elsevier Science Limited.*

1 Introduction

The great weakness of monolithic ceramics is their intrinsic inability to tolerate mechanical damage without brittle rupture because of their polycrystalline state and the nature of the chemical bonds existing in these compounds. The use of long, woven ceramic fibres embedded in a refractory ceramic matrix can result in a metastable composite material exhibiting greater toughness through a specific micromechanism at the fibre–matrix interface: the matrix cracking can be deflected, dissociated and even arrested when a propagating crack meets the reinforcing fibres and thus composite materials can exhibit a fibrous, pseudo-plastic fracture.[1]

One of the main problems in the preparation of ceramic matrix composites is to achieve a low open porosity in the matrix. The fibres must be thoroughly embedded in the matrix and the matrix precursor must be incorporated through the voids between fibres (a few microns or less, in size). This is only possible by infiltration of liquid or gaseous precursors for which the ceramic yield is necessarily low, which implies porosity and cracks. The latter method is used for the synthesis of covalent bonded ceramics of a rather simple composition (e.g. C, SiC, BN, ...)[2] whereas the former is more versatile (for SiC, Si_3N_4, various multicomponent oxides, ...).[3,4] The liquid precursor is a slurry of submicron powder or a metal-organic reagent (alkoxide, ester, polysiloxane, polysilazane, ...)[3,4] leading after pyrolysis to oxide, carbide, nitride, ... In both cases, there is considerable shrinkage after pyrolysis which produces new voids; however, the presence of the woven fabrics can efficiently inhibit the coherent shrinkage of the matrix. In the case of one- or two-dimensional reinforcements, this dilemma is solved by the hot pressing of impregnated and coated fabrics[5,6] To solve this problem is more complicated when a three-dimensional (3D) reinforcement is used. The 3D interconnected array of fibres segments the matrix, which cracks when sintering takes place. Thus, the methods based on the slow condensation of gaseous precursor (Chemical Vapour Infiltration (CVI) is commonly used. This paper will demonstrate how the post-infiltration of a specified ceramic precursor—and its *in situ* pyrolysis—between the primary infiltrated powder particles by pressure-assisted infiltration can improve the mechanical strength of 3D fibre reinforced ceramic matrix composites and that liquid precursors offer an alternative method of preparing 3D reinforced ceramic matrix composites (CMCs).

Various sol–gel precursors leading to inert refractory non-reacting interphase (Zr-i-propoxide as zirconia precursor, Al-butoxide as alumina precursor), reacting interphase (Ti-i-propoxide as rutile precursor, tetraethoxysilane (TEOS) as silica precursor) or bloating interphase (Al–Si ester, as aluminosilicate precursor) have been considered in

*Corresponding author, also at CNRS, LASIR, 2 rue Henri Dunant, 94320 Thiais, France.

association with a primary matrix made of infiltrated alumina powder.

The idea of using liquid ceramic precursors for the consolidation of a fibre preform originates from the processing route used for C/C composites (infiltration of pitch or of phenolic resin). Similar routes have been tested for the preparation of SiC matrix composite using polysilane precursors.[7,8] Preparation of composite materials by infiltration of oxide porous bodies with organic metallic reagents has been recently discussed by Honeyman-Calvin and Lange,[9] but the case of oxide matrix 3D fibre reinforced bodies has not been considered except for the experimental details given in our patent.[10]

2 Experimental Procedure

Figure 1 shows a schematic of the two-step infiltration process. The first step (stages 1 and 2) consists in the preparation of a powder compact within the fibre preform by slip-cast infiltration (stage 1), the specimen being dried and then strengthened by heating (stage 2). The second step consists in the infiltration of the strengthened body with a liquid precursor (stage 3) that is converted into a gel by reaction with water (or diols) (stage 4) and then into a refractory phase during pyrolysis (stage 2). The second step can be repeated many times.

2.1 3D preform

The carbon fibre preform consists of sheets of felted fibres which are sewn along the third dimension, with the same kind of fibre (Novoltex® from SEP, Le Haillan, 33165 Saint Médard en Jalles, France). This linkage is obtained by passing fibre thread through the sheets to form stitches. The fibre volume fraction is ~28%. The fibre diameter ranges between 7 and 10 μm. The 8-mm thick preform is cut to form a 40 mm × 120 mm plate.

2.2 Powder and slurry

A submicron powder (AKP50 from Sumitomo) consisting of spherical, well-crystallized α-alumina particles, of mean diameter 0·1–0·3 μm and specific area 10 m^2/g, is used as the matrix starting material. A 300 g/litre alumina slurry is prepared by dispersion in water with addition of nitric acid (pH = 4), with the help of mechanical and ultrasonic stirring for 1 h. Aggregates larger than 0·6 μm are eliminated by overnight sedimentation. Ultrasonic mixing is carried out for 15 min just before use. The aggregate size distribution is checked using a HORIBA CAPA 700 size analyser.

2.3 Monoliths and composites

The slurry is slip-cast under 2 MPa air pressure through the fibre preform plate using the technique previously described by Jamet *et al.*[11] A filter paper under the preform plate is used to retain the thinner particles inside the preform (Fig. 1). A drilled aluminium plate acts as a mechanical support. Nevertheless, some of the first particles with mean diameter below 0·05 μm are not retained in the preform. A vacuum is applied under the filter paper support to promote rapid slip-casting (<2 h). Then, the infiltrated

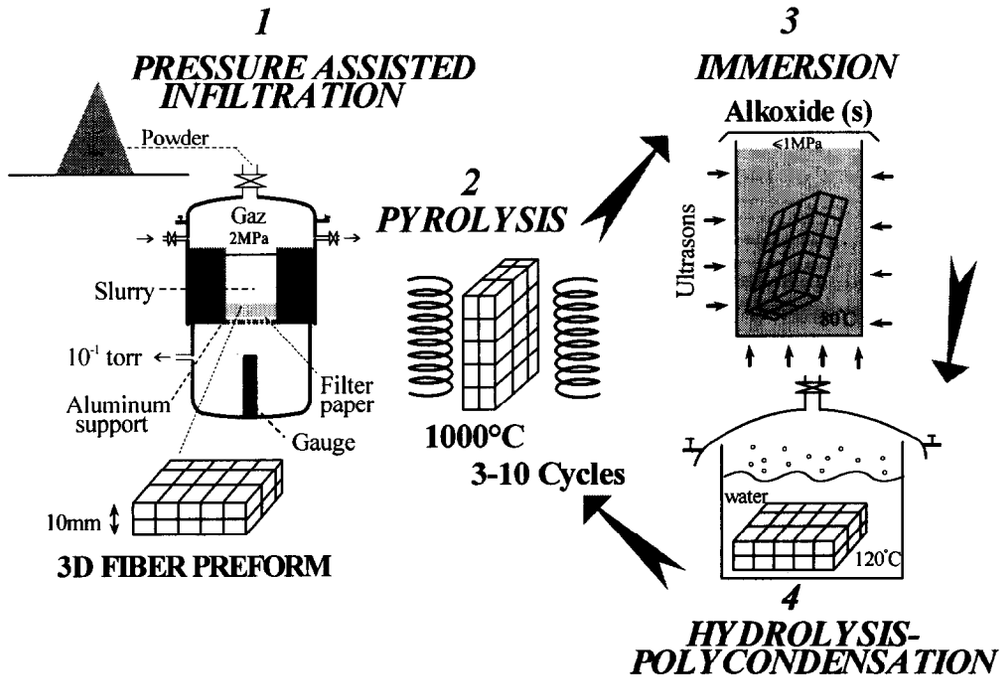

Fig. 1. Flow diagram of two-step infiltration process, first using a pressure-assisted slip-casting infiltration device and second by *in situ* hydrolysis-polycondensation of a specific interphase precursor.

preform is dried stepwise in a controlled humidity atmosphere at selected temperatures between 40 and 120°C. The drying time is 15 h.

Monoliths are processed without the fibre preform plate, and the powder particles are retained by the sole filter paper. Dried monoliths with 60% of the theoretical density for α-alumina can be achieved.

The infiltrated preform and monoliths are thermally treated at selected temperatures between 1000 and 1400°C in a reducing argon atmosphere for 1 h in a carbon resistance furnace.

2.4 Microstructure and mechanical characterization

Monolith shrinkage was recorded versus temperature using an Adamel Lhomargy DI24 apparatus (Instrument SA, 91 Longjumeau, France) with an alumina rod and support (heating/cooling rate: 5°C/min). The pore size and distribution are measured by mercury infiltration using a Micromeritics Pore Sizer 9310 according to the ASTM vol. 1201, C699-1983 notice. The validity of the measurement has been verified by calibration of the mercury/composite surface angle by comparison with the pore volume determined using N_2 adsorption/desorption plots carried out with a Micromeritics ASAP2000 instrument. Comparable results are obtained for a surface angle equal to 145°, this value being intermediate between the angle values commonly used for Hg/C (155°) and Hg/oxide (130°) interfaces. The open porosity has been calculated according to Archimedes' method. The flexural strength was recorded by a three-point bending test using specimens of 40 mm × 8 mm × 2 mm at a cross-head speed of 0·1 mm/min at room temperature and at 1200°C (1300°C) under argon, with 1 h stabilization at the temperature of measurement. The tensile strength was recorded at room temperature on a dumbbell specimen machined in a 120 mm × 40 mm × 8 mm composite using a 10 μm deformation gauge.

3 Results and Discussion

3.1 Matrix shrinkage and its influence on mechanical properties

Dilatometric traces of the slip cast monoliths from AKP50 suspensions show that sintering starts at 1000°C and ends at 1450°C.[12] (The bending ultimate strength can reach 400 MPa for the monolith specimen sintered at 1400°C). The nil dilatation/shrinkage point is observed at 1100°C. Consequently, microcracking and a fibre–matrix gap are observed in the composite heated above 1100°C, and the presence of the 3D geometric invariant fibre preform promotes the segmentation of the matrix. A typical example is shown in Fig. 2. This phenomenon lowers the mechanical strength. The improvement to the thermomechanical properties can be achieved if (i) net-shape shrinkage is obtained, (ii) the porosity is decreased and (iii) the mechanical strength of the bulk matrix is increased without the formation of a strong fibre-matrix interface.

At temperatures ranging from 1000 to 1400°C, the sintering of an alumina submicron powder takes place by solid-state diffusion at the particle contacts. The interposition of an inert second phase between particles would prevent, or reduce, the formation of the contact for solid-state diffusion. The interparticle voids could also affect shortening of the interparticle distance during sintering.

The high green density of the monolith sample (60% of the theoretical density) indicates a highly optimized packing of the AKP50 particles. The open porosity of monoliths thermally treated at 1000°C ranges from 34 to 36% and that of composites with the 3D preform (carbon fibre volume fraction: 28%) ranges from 35 to 38%. This indicates that the AKP50 particle packing inside the preform is rather similar to that in the monolith. Figure 3(a) compares the pore volume distribution in the monolith alumina sample with that in the composite heated at various temperatures. Only one family of pores (mean diameter ~0·05 μm) is observed in the monolith alumina sample. This pore range corresponds well to the voids between adjacent AKP50 particles. It is noted that the pore volume ranges up to 0·01 μm for the monolith alumina sample heated below 1200°C, according to its shrinkage. On the other hand, three kinds of porosity are observed in the composite:

(i) The first family, centred near 0·05–0·1 μm, is assigned to the interparticle voids as observed in the monolith alumina sample. The small shift toward high values indicates that the packing is slightly disturbed by the 3D fibre network.
(ii) A broad distribution from 0·2 to 10 μm can be assigned to the voids between fibres (infiltrated powder can be lacking from bundles, as evidenced by microscopy) and to voids between fibres and matrix particles, the latter voids increasing with increase in thermal treatment temperature.
(iii) A bimodal distribution between 10 and 20 μm is assigned to cracks originating from constricted shrinkage, as shown in Fig. 2.

Increasing the sintering temperature led to narrowing of the pore size in the monolith, resulting from particle centre shortening and pore collapsing

which took place after sintering at 1300°C. The same phenomenon occurred for the composite matrix but cracks dominated after sintering at 1300°C due to the matrix segmentation imposed by the invariable fibre array: the matrix densification created cracks.

The low viscosity (~0·5–1 poise) of the liquid polymeric precursors[10] makes it possible to infiltrate them in porous ceramics and to convert them into ceramics by 'polymerization' and then pyrolysis. Hydrolytic polycondensation of alkoxides is well documented for the preparation of oxides.[13–16]

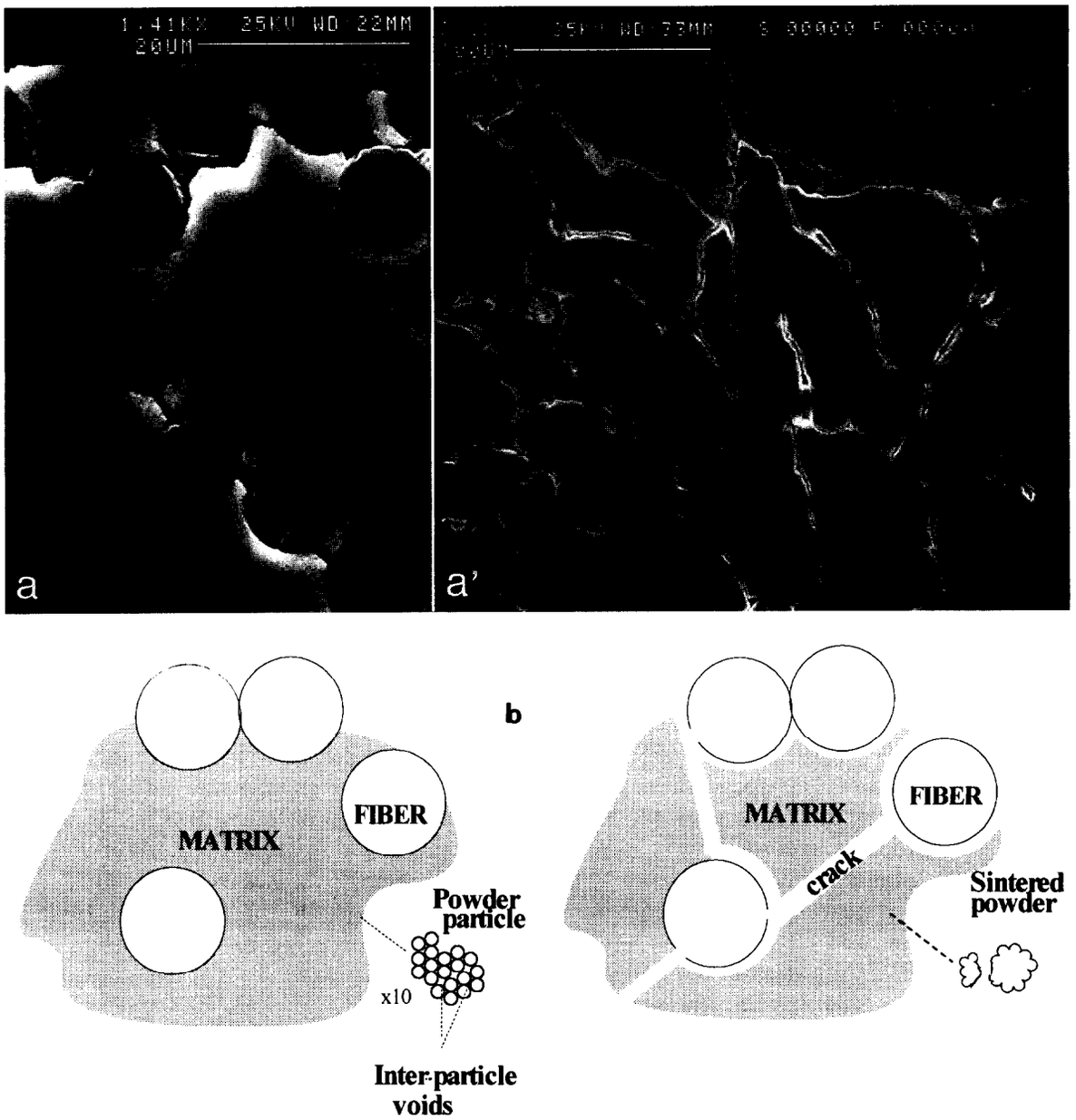

Fig. 2. Microphotographs of a 1200°C sintered composite (a, bar: 20 μm; a', bar: 100 μm). The microcracking induced by the competition between the matrix shrinkage and the invariant 3D fibre network is sketched in (b); detail of the dense packing of primary oxide particles with inter-particle voids available for alkoxide infiltration is shown.

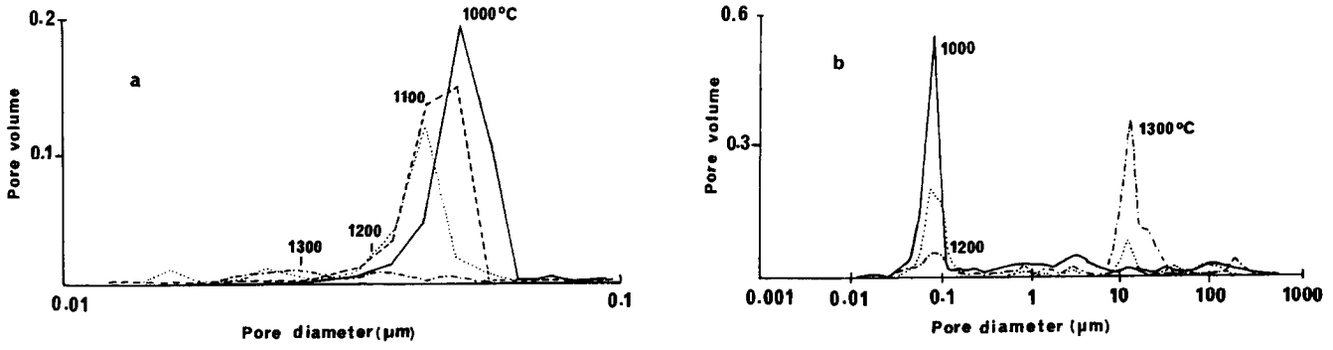

Fig. 3. Pore distribution in an alumina monolith (a) and in a 3D reinforced composite (b), versus sintering temperature.

Among commercially available reagents, we have selected titanium butoxide ($Ti(OC_4H_5)_4$), aluminium s-butoxide ($Al(OC_4H_5)_3$*, TEOS ($Si(OC_3H_5)_4$), aluminium–silicon ester ($(OC_4H_5)_2$-Al-O-$Si(OC_3H_5)_3$) and zirconium i-propoxide ($Zr(OC_3H_7)_4$); the high melting temperature of the corresponding oxides may exclude a strong reaction with alumina below 1400°C. Furthermore, their viscosity can be adjusted at about 0·7 poise by heating between 40 and 80°C.[10] Hydrolysis-polycondensation and drying at 150°C leads to gels with the following typical formula: $TiO_{1.5}(OH).5H_2O$, $ZrO_{1.98}(OH)_{0.04}.4H_2O$ and $Al_2O_{2.7}(OH)_{0.6}.5H_2O$.[17,18]

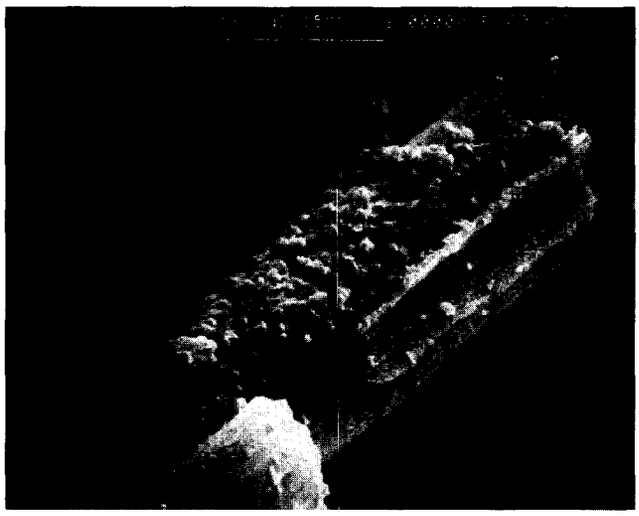

Fig. 4. Zirconia deposit at surface of a C fibre (diameter ~9 μm) observed in the fracture of a 1200°C heat-treated composite after eight infiltration cycles of zirconium i-propoxide.

3.2 Alkoxide infiltration and pyrolysis

The infiltration has been detailed in our patent.[10] Samples (i.e. the strengthened powder compacts, stage 2 of Fig. 1) are carefully dried at 200°C, then immersed in liquid alkoxides (under atmospheric pressure or 1 MPa) for 30 min with the help of ultrasonic stirring (stage 3); next they are immersed in boiling water at 120°C for 3 h (stage 4) then finally dried at ~120°C and pyrolysed at various temperatures from 1000 to 1400°C (stage 2). Typically 2–3% of the porosity is filled by oxide after one cycle.[12] Figure 4 shows an example of the deposition on the fibre, which was obtained from the alkoxide hydrolysis-polycondensation inside the composite. The small agglomerates (mean diameter ≤0·5 μm) after pyrolysis are visible. Analysis of the zirconium concentration across the monolith thickness after four cycles of infiltration and pyrolysis reveals a higher concentration zone in the vicinity of the monolith surface. This gives a laminar behaviour to the monolith (Fig. 5). The location of high zirconia content regions after infiltration seems to be related to the pore heterogeneity resulting from slip-casting.

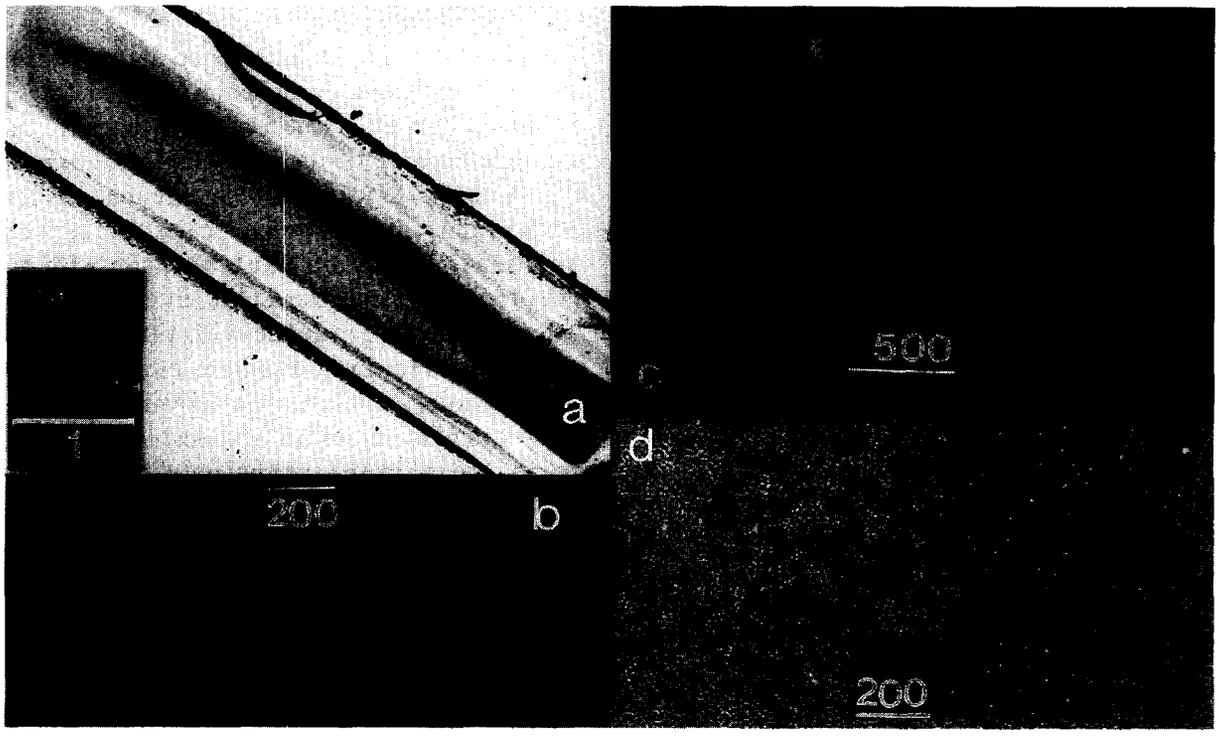

Fig. 5. Back-scattered electron micrograph of an alumina monolith after four cycles of zirconium i-propoxide infiltration-hydrolysis firing and final heat treatment at 1400°C in air (a, bar: 10 mm). Detail at larger magnitude is given in (b, bar: 20 μm) and (c, bar: 500 nm). A SEM micrograph of the frontier between the dense core and the porous contour is given in (d, bar: 200 μm).

*This reagent must be handled in a glove box (≤10 p.p.m. H_2O) and careful drying of the porous materials to be infiltrated is required.

Examination of the monolith shows a porous region below the upper surface. After 10 cycles of infiltration-thermal treatment at 1000°C, the open porosity is typically 24% using simple capillarity intrusion and 20% using pressure-assisted infiltration. Full densification is obtained after a 1400°C thermal treatment for 1 h. Figure 5(c) shows that the oxide particles resulting from the gel pyrolysis are homogeneously dispersed and form particles with 0·2 μm mean diameter which corresponds well to the size of interparticle voids. Consequently the flexural strength measured at room temperature reaches 550 MPa.

The evolution of the pore volume distribution as a function of size for various thermal treatments shows that the mean pore size of a monolith post-infiltrated with a zirconia gel first increases up to 1200°C and then decreases (Fig. 6(a)). This agrees with the lack of shrinkage up to 1300°C. The infiltration yield is a maximum for materials infiltrated with aluminium s-butoxide pyrolysed at 1200°C (Fig. 6(b)). On the other hand, the highest yield is observed for materials infiltrated with zirconium propoxide pyrolysed below 1100°C. This phenomenon can be related to the high reactivity of aluminium s-butoxide versus water. The surface of alumina porous bodies heated below 1200°C easily retains water molecules. Uncontrolled hydrolysis leads to pore clogging and hence decreases the infiltration yield. Comparison of the dilatometric traces of the same monolith shows that the linear shrinkage after 1400°C thermal treatment is reduced from 12 to 5% after only one cycle of infiltration with zirconium i-propoxide. A net-shape consolidation is obtained up to 1300°C. Figure 7 gives a comparison between the pore volume distribution measured for a composite without and after eight cycles of zirconium i-propoxide infiltration-hydrolysis-polycondensations and 1200°C firing. The lack of voids generated by matrix cracking in the post-infiltrated alumina matrix composite is straightforward in the pore diameter distribution (Fig. 7).

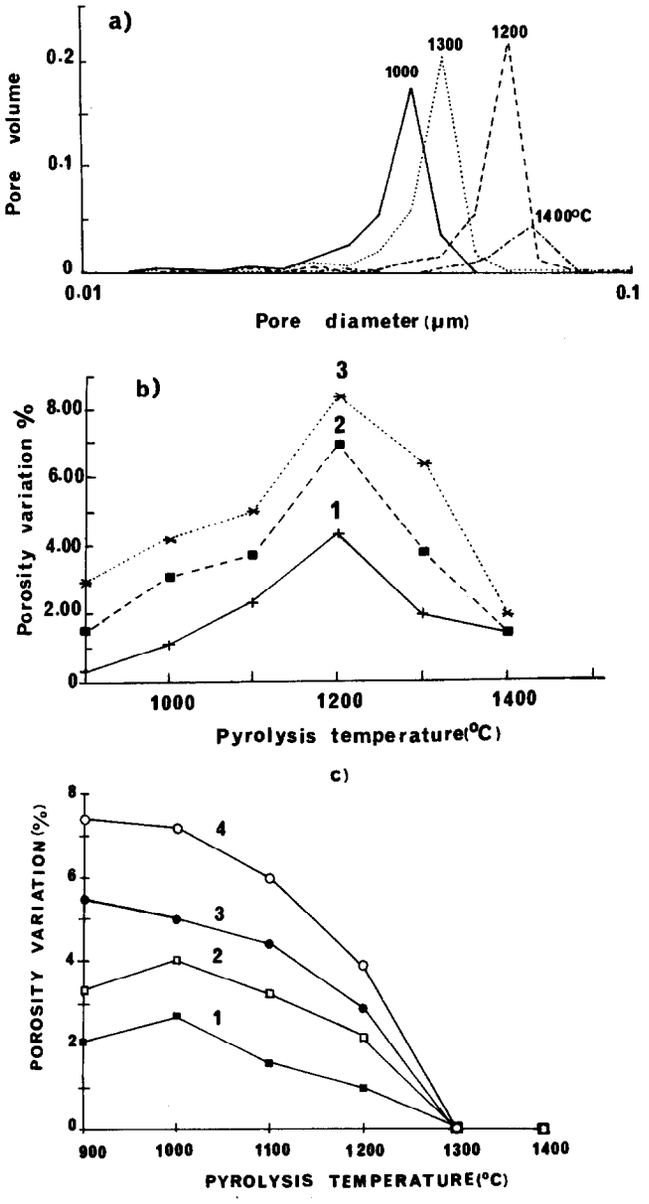

Fig. 6. Evolution of pore diameter distribution as a function of sintering temperature for a monolith after four cycles of zirconium i-propoxide post-infiltration and *in situ* hydrolysis-polycondensation (a); cumulative porosity variation for an alumina monolith post-infiltrated with aluminum s-butoxide (b) and zirconium propoxide (c) and pyrolysed at various temperatures (1: first cycle, 2: second cycle, 3: third cycle, ...).

3.3 Optimization of the post-infiltrated interphase precursor

Post-infiltration with a liquid precursor of a very refractory composition allows the prevention of interparticle diffusion and hence matrix shrinkage by the formation of an interphase acting as a diffusion barrier. However, this barrier cannot continue because of the low yield of ceramization: Fig. 4 shows cracks between zirconia aggregates (<0·05 mm) and between scales of aggregates. Additional infiltration must be made with a precursor which strengthens the interparticle bond. Attempts have been made with titanium alkoxide infiltration. However, titanium ethoxide (propoxide, butoxide, ...) infiltration activates the sintering of an alumina monolith and segmentation of the matrix occurs in the composite. Consequently the mechanical properties remain poor. The net-shape temperature (nil expansion/shrinkage) on the dilatometric trace occurs at 1050°C and the final linear shrinkage of 1400°C heat-treated rutile precursor infiltrated monolith reaches 14% instead of 12% for a pure AKP50 monolith. The origin of this sintering activation can be found in the easy diffusion of titanium in alumina.

Figure 8 shows the dilatometric trace of aluminosilicate gel prepared by hydrolysis-polycondensation of aluminium–silicon ester *in vacuo*. Marked expansion occurs above 1200°C. This phenomenon,

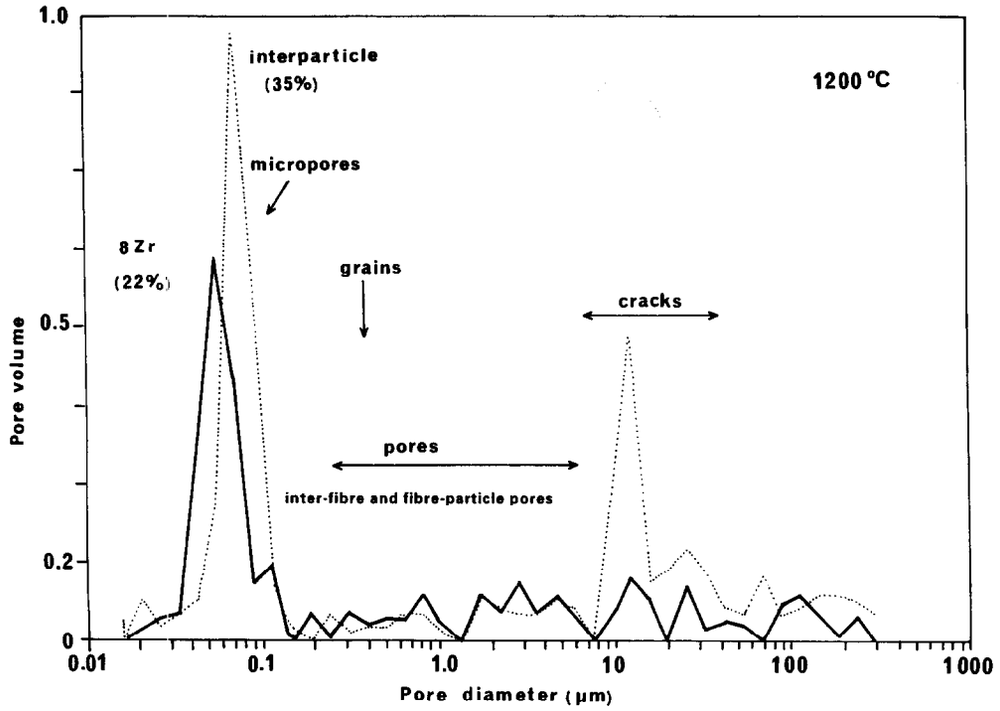

Fig. 7. Comparison of pore diameter distribution for a composite without (dotted line) and with eight cycles of zirconium i-propoxide post-infiltration and subsequent *in situ* hydrolysis-polycondensation (solid line). Thermal treatment was made at 1200°C. Assignment of the different kinds of pore is given.

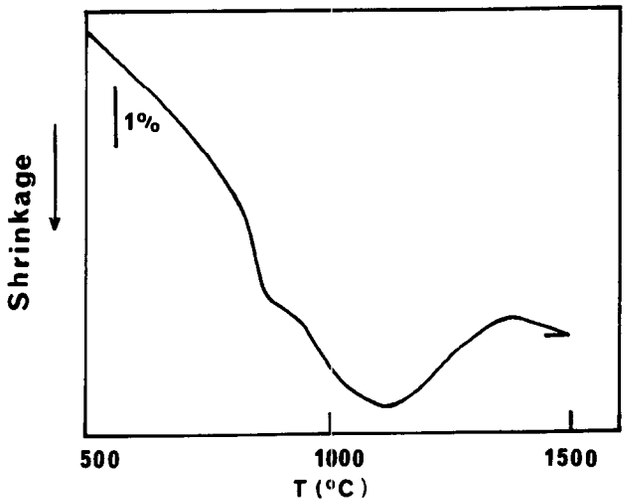

Fig. 8. Shrinkage expansion of aluminosilicate xerogel from aluminium–silicon ester heated in vacuum reducing atmosphere.

which is related to gas evolution (H_2O and CO) owing to the final dehydroxylation and to the oxidation of carbon residues, is observed when, simultaneously, the viscosity is lowered.[19] Post-infiltration with this precursor may promote good interparticle bonding without shrinkage.

3.4 Mechanical properties

Figure 9 shows typical flexural stress–strain plots recorded for composites before and after post-infiltration. A significant increase in the strength is observed at temperatures up to 1300°C. The ultimate flexural strengths measured at room temperature, 1200°C and 1300°C are compared in

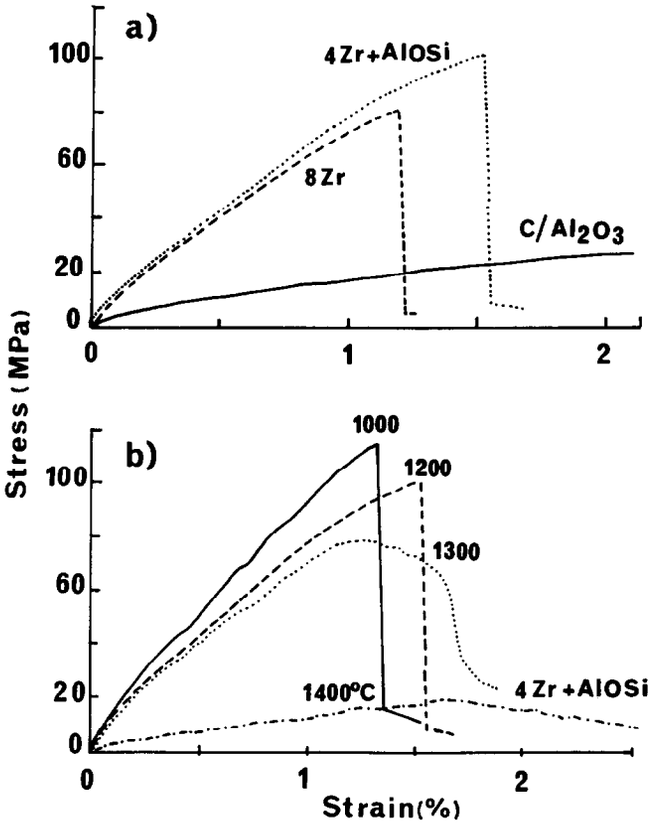

Fig. 9. Room temperature flexural stress–strain traces (a) for a C/Al_2O_3 composite before and after eight cycles of zirconium i-propoxide post-infiltration, *in situ* hydrolysis-polycondensation (HP) and 1000°C firing (8Zr) and after four cycles of zirconium-propoxide post-infiltration and HP and 1000°C firing with a subsequent infiltration cycle using aluminium–silicon ester (4Zr+AlOSi). The stress–strain traces recorded for this last sample sintered at various temperatures are given in (b).

Fig. 10(a), and the use of four zirconium propoxide infiltrations followed by one infiltration with aluminium–silicon ester appeared an effective combination both for the fabrication of the composites (handling in air) and for strength. It is noticed that the strength at room temperature is lower than that at high temperatures. Self-healing could occur at high temperature between the aluminosilicate interphases derived from the (aluminium) silicon alkoxide precursor at high temperatures. A typical tensile stress–strain plot recorded at room temperature is given in Fig. 10(b) and the hysteresis indicates the loading–unloading cycle. The same phenomenon has been observed for SiC matrix composites prepared using the pyrolysis of infiltrated polysilazane precursor in the 3D composite.[8,19] On the other hand, the SiC matrix composites processed using the CVI route do not exhibit such hysteresis. The difference can be related to the meso/microporosity of the matrix in the composites derived from pyrolysed metal-organic reagent from which the solids yield is low (~25–30% for alkoxides). The homogeneity of this meso/micro-porosity can help to accommodate, by microcracking, the thermal stress from thermal expansion mismatch but lowers the Young's modulus. For instance, the tensile Young's modulus of post-infiltrated alumina matrix composites, prepared from the same 3D fibre preform, ranges between 20 and 30 GPa, whereas that of the SiC matrix composite processed by the CVI route is 75 GPa.[20] Thus, the mechanical properties of CVI processed composites are significantly sensitive to thermal cycling. Composites prepared from liquid oxide precursor might not be sensitive to the thermal cycling, but the low rigidity of their matrix prevents their use under tensile-compressive cycling as established for the SiC matrix composites.[20] Nevertheless, post-infiltrated oxide matrix composite and CVI SiC matrix composite exhibit the same mechanical strengths.

4 Conclusions

This novel processing route using the liquid infiltration cycles, i.e. first using a suspension of a submicron alumina powder, then using an alkoxide (or any liquid precursor) offers several advantages: controlling the matrix shrinkage during sintering to avoid matrix segmentation in 3D preform, controlling the interparticle chemical bonding to strengthen the interparticle bonding without shrinkage and simplifying the process.

The mechanism whereby composites have a higher strength at high temperatures is believed to be the reaction between the aluminosilicate interphase derived from the alkoxide by the last post-infiltration and the primary alumina matrix, the matrix shrinkage being simultaneously hindered by the initial post-infiltration of a zirconia intergranular phase.

Acknowledgement

Thanks are due to the Société Européenne de Propulsion (SEP), Le Haillan, 33165 Saint Médard en Jalles, for supporting M. Wey financially.

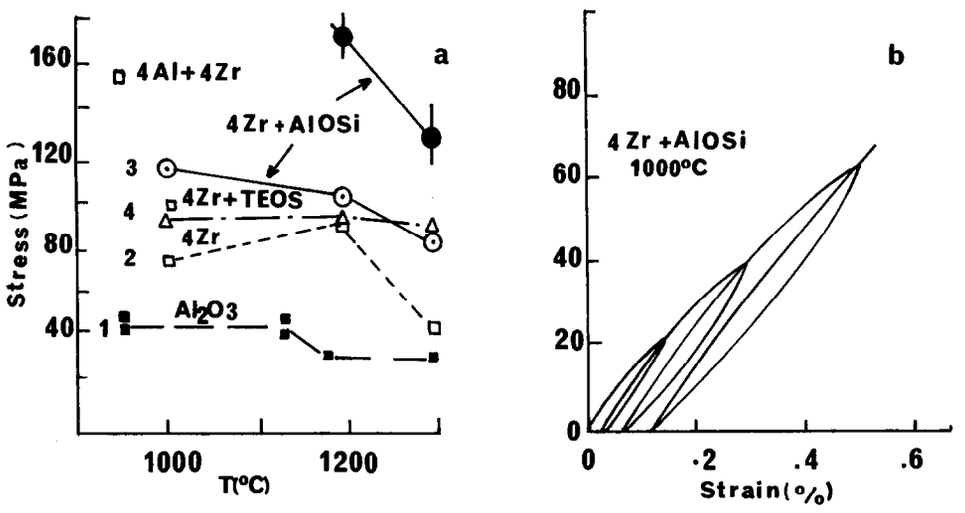

Fig. 10. Room-temperature flexural strength versus deformation of a composite before (CAl_2O_3) and after post-infiltration and *in situ* hydrolysis-polycondensation and subsequent sintering at various temperatures: four infiltrations with zirconium i-propoxide (4Zr), with additional TEOS (4Zr+TEOS) or aluminium–silicon ester (4Zr+AlOSi) post-infiltration or alternatively, zirconium i-propoxide and aluminium s-butoxide (4Al+4Zr) post-infiltrations have been successively made. Black circles correspond to data recorded at the temperature given by the abscissa, in argon atmosphere, after one hour stabilization at high temperature for 4Zr+AlOSi post-infiltrated composites. The corresponding room-temperature tensile strain–stress plot is given for a 4Zr+AlOSi composite sintered at 1000°C (three loading/unloading cycles have been made before the rupture).

References

1. Aveston, J., Cooper, G. A. and Kelly, A., In *Proc. Conf. on the Properties of Fiber Composites*, National Physical Lab., 4 November 1971, London. IPC Sci. and Tech. Press Ltd, Guilford, Surrey, 1971, pp. 15–26.
2. Naslain, R. and Langlais, F., CVD processing of ceramic–ceramic composite materials. In *Tailoring Multiphase and Composite Ceramics*, Mat. Sci. Res., Vol. 20. Plenum Press, New York, 1985, pp. 145–164.
3. Lamicq, P. J., Bernhart, G. A., Dauchier, M. M. and Macé, J. G., SiC/SiC composite ceramics. *Am. Ceram. Bull.*, 1986, **65**(2), 336–338.
4. Colomban, Ph., Process for fabricating a ceramic matrix composite incorporating woven fibers and materials with different compositions and properties in the same composite. *Mater. Technol.*, 1995, **10**(5/6), 93–96.
5. Colomban, Ph., Bruneton, E., Lagrange, J. L. and Mouchon, E., Sol–gel mullite matrix-SiC and -mullite 2D woven fabric composites with or without zirconia containing interphase. Elaboration and properties, *J. Eur. Ceramic Soc.*, 1996, **16**(2), 301–314.
6. Mouchon, E. and Colomban, Ph., Oxide ceramic matrix–oxide fibers woven fabric composites exhibiting dissipative fracture behavior. *Composites*, 1995, **26**, 175–182.
7. Parlier, M., Bouillon, E., Muller, C., Bloch, B., Noireaux, P. and Jamet, J., Procédé d'élaboration d'un matériau composite céramique fibres–matrice et matériau composite obtenu par ce procédé. ONERA French Patent No. 8916918 (20/12/1989).
8. Sudre, O., Parlier, M. and Bouillon, E., Comparative mechanical evaluation of two 2.50 C/SiC composites processed via chemical vapor infiltration and powder/polymer injection route. *Proc. 2nd Int. Conf. on High-Temperature Ceramic Matrix Composites HT-CMCII*, Santa-Barbara, 21–24 Aug. 1995, Vol. I, Ceram. Trans. 58, ed. R. Naslain and A. G. Evans. Am. Ceram. Soc., Westerville, 1995, pp. 13–18.
9. Honeyman-Calvin, P. and Lange, F. F., Infiltration of porous alumina bodies with solution precursors: strengthening via compositional grading, grain size control and transformation toughening. *J. Am. Ceram. Soc.*, 1996, **79**(7), 1810–1814.
10. Colomban, Ph., Wey, M. and Parlier, M., Procédé d'élaboration d'un matériau céramique par infiltration d'un précurseur dans un support poreux céramique. ONERA French Patent No. 2713222 (9/6/1996).
11. Jamet, J., Demange, D. and Loubeau, J., Nouveaux matériaux composites alumine–alumine à rupture fortement et leur préparation. ONERA French Patent No. 2526785 (18/11/1983).
12. Wey, M. and Colomban, Ph., Densifier sans retrait: une nécessité pour l'optimisation des propriétés mécaniques de composites céramiques 3D satisfaits par la polymérisation *in situ*. *Proc. JNC10, 10èmes Journées Nationales sur les Composites*, Paris, 29–31 Octobre 1996, ed. D. Baptiste and J. Vautrin. AMAC, Paris, 1996, Vol. 3, pp. 1133–1142.
13. Klein, L .C. (ed.), *Sol–gel Technology*. Noyes Publ., Park Ridge, N.J., 1988.
14. Colomban, Ph., Gel technology in ceramics, glass–ceramics and ceramic–ceramic composites. *Ceramics Int.*, 1989, **15**, 23–50.
15. Pierre, A. C., *Introduction aux Procédés Sol–Gel*. Editions Septima, Paris, 1992.
16. Segal, D., *Chemical Synthesis of Advanced Ceramic Materials*. Cambridge University Press, Cambridge, 1989.
17. Bruneton, E. and Colomban, Ph., Influence of hydrolysis conditions on crystallisation, phase transition and sintering of zirconia prepared by alkoxide hydrolysis. *J. Non-Crystalline Solid*, 1992, **147&148**, 201–205.
18. Colomban, Ph. and Vendange, V., Sintering of alumina and mullite prepared by slow hydrolysis of alkoxides: the role of the protonic species and of pore topology. *J. Non-Crystalline Solid*, 1992, **147&148**, 245–250.
19. Bruneton, E., Bigarré, J., Michel, D. and Colomban, Ph., Heterogeneity, nucleation, shrinkage and bloating in sol–gel glass–ceramics. *J. Mater. Sci.*, **32**, in press.
20. Parlier, M. and Colomban, Ph., Composites à matrice céramique pour applications thermostructurales. *La Recherche Aérospatiale*, 1996, **5/6**, 457–469.